Self and N2 collisional broadening of far-infrared methane lines at low-temperature with application to Titan

C. Richard, V. Boudon, L. Manceron, J. Vander Auwera, S. Vinatier, B. Bézard, M. Houelle

Self and N_2 collisional broadening of far-infrared methane lines at low-temperature with application to Titan.

C. Richard[a,*], V. Boudon[a], L. Manceron[b,c], J. Vander Auwera[d], S. Vinatier[e], B. Bézard[e], M. Houelle[e,f]

[a]*Laboratoire Interdisciplinaire Carnot de Bourgogne, UMR 6303 CNRS - Université Bourgogne Franche-Comté, 9 Av. A. Savary, BP 47870, F-21078 Dijon Cedex, France*
[b]*AILES, Synchrotron SOLEIL, L'Orme des Merisiers Saint-Aubin, F-91192 Gif-sur-Yvette, France*
[c]*LISA, Université Paris Cité and Univ Paris Est Creteil, CNRS, LISA, F-75013 Paris, France*
[d]*SQUARES, C.P. 160/09, Université Libre de Bruxelles, B-1050 Brussels, Belgium*
[e]*LESIA, Observatoire de Paris, Université PSL, Sorbonne Université, Université Paris Cité, CNRS, 5 place Jules Janssen, 92195 Meudon, France*
[f]*Observatoire de Genève, Université de Genève, Chemin Pegasi 51, 1290 Sauverny, Switzerland*

Abstract

We report the measurement of broadening coefficients of pure rotational lines of methane at different pressure and temperature conditions. A total of 27 far-infrared spectra were recorded at the AILES beamline of the SOLEIL synchrotron at room-temperature, 200 K and 120 K, in a range of 10 to 800 mbar. Self and N_2 broadening coefficients and temperature dependence exponents of methane pure rotational lines have been measured in the 73–136 cm^{-1} spectral range using multi-spectrum non-linear least squares fitting of Voigt profiles. These coefficients were used to model spectra of Titan that were compared to a selection of equatorial Cassini/CIRS spectra, showing a good agreement for a stratospheric methane mole fraction of (1.17 ± 0.08)%.

Keywords: Methane, Synchrotron radiation, Far-infrared, Pressure broadening, Titan, Cassini/CIRS

1. Introduction

Methane is an important molecule for the study of planetary atmospheres. It is present in many planets and bodies of the Solar System, but it is also found, at high temperature, in the atmosphere of several exoplanets. The study of methane lines at low temperature, as in this study, is of great interest to probe the thick atmosphere of Titan [1] but also of ice giants. It has for example been used to measure the spatial distribution of methane in the stratosphere of Titan from the Cassini Composite InfraRed Spectrometer (CIRS) spectra [2], showing here the importance of close-up observations. Although since 2018 no more spacecraft are into orbit around the Saturnian system, Dragonfly is a planned NASA mission [3] which is expected to land on Titan in 2034, bringing to its surface a robotic rotorcraft. Moreover, interest in ice giants has been renewed recently with a proposed mission that plans to send a spacecraft into orbit

*Corresponding author
Email address: Cyril.Richard@u-bourgogne.fr (C. Richard)

around Uranus together with a descent probe, scheduled for launch in 2031 or 2032 [4]. This planet is known to have methane clouds at a temperature of about 100 K [5] showing again the interest to study the broadening of the methane lines at such temperatures. Methane has also been observed in Neptune's stratosphere [6] and has been extensively analyzed with the PACS instrument onboard the *Herschel* telescope [7].

However, in the atmospheric environments, methane is generally mixed with other gases, like nitrogen in Titan's case. It is therefore essential to also study the broadening of methane lines in a medium diluted with nitrogen in order to take into account all collision broadening effects.

Section 2 details the experimental setup and the conditions used to record the spectra at the synchrotron facility SOLEIL. The measurements of nitrogen-broadening coefficients and temperature dependence exponents, and details on the fitting procedure are described in Section 3 and Section 4. Section 5 is a discussion of our results and compares them with values found in HITRAN and other references. Finally, we applied these results to an analysis of methane rotational lines observed on Titan in Section 6 and present our conclusions in Section 7.

2. Experimental details

To estimate the temperature dependence of the broadening coefficients of the very weak pure rotation lines of methane [8], a wide range of temperature and pressure conditions combined with a long optical path length were required. Absorption spectra were therefore recorded on the AILES Beamline at the SOLEIL synchrotron facility (Saint-Aubin, France), with the synchrotron light source coupled to a Bruker IFS 125HR Fourier transform spectrometer [9, 10], maintained at 4×10^{-5} mbar, and the AILES cryogenic long path cell [11]. A total of nineteen high-resolution spectra were recorded at low-temperature with an optical path length of 93.14(1) m. For the new spectra the iris was set to 2.5 mm, while for the older spectra, the iris was open to it's maximum value of 12.5 mm. In any case, the effective size of the source at the spectrometer entrance was smaller than the maximum size required for the highest resolution at the useful wavenumbers. The unapodized spectra were obtained in the 40–300 cm^{-1} region at resolutions varied from 0.05 to 0.001 cm^{-1} (defined as 0.9/maximum optical path difference, see Table 1), with a 3.8 cm/s scanner velocity, a 6 µm Si/Mylar beamsplitter and a 4 K-cooled Si composite bolometer with a 1.5 ms rise time and a cold 300 cm^{-1} low-pass filter. The recorded spectra result from the co-addition of various numbers of interferograms (see Table 1). They were divided by low resolution (0.05 cm^{-1}) empty cell spectra taken at the same temperature. The resulting transmittance spectra were zero-filled, corrected for channelling effects and calibrated using well-known water rovibrational lines [12] with a standard deviation of about 3×10^{-4} cm^{-1}.

Two series of low-temperature measurements were carried out specifically for this study (Table 1), while spectra at room temperature were recorded previously by Sanzharov et al. [13] and are not reported in this study. For all these spectra, the synchrotron radiation from the SOLEIL facility (500 mA in the most stable operation mode with 316 equally filled electron bunches, 430 mA for spectra 4 and 5) was used as a source. Spectra 4 and 5, with the highest pressures of pure methane, were recorded in a first series at an earlier date. For these measurements, the objective mirrors were slightly warmed by specific heaters to keep mirror actuators from jarring, and this resulted in a larger pressure gradient which is responsible for relatively large temperature error bars. In a second measurement series at a later date (spectra 1-3 and 6-19), this effect could be drastically reduced and the uncertainties from the temperature gradient are reduced by a factor of two. Uncertainty on methane or nitrogen broadening gas pressures is always smaller than 0.5%.

Table 1: Experimental conditions for the low-temperature CH_4 spectra recorded in this study.

Spectrum	CH_4 Pressure[a] / mbar	Temperature[a] / K	# Averaged scans	Resolution / cm^{-1}	Pressure N_2[a] / mbar
1	10.67(5)	120(4)	336	0.001	0
2	20.4(1)	120(4)	320	0.002	0
3	41.7(2)	125(4)	256	0.004	0
4	50.0(3)	129(10)	578	0.005	0
5	100.1(5)	117(10)	320	0.01	0
6	21.3(1)	124(4)	1000	0.005	79.5(4)
7	41.7(2)	125(4)	320	0.008	159.0(8)
8	80.0(4)	120(4)	1060	0.02	320(2)
9	79.5(4)	125(4)	320	0.01	80(4)
10	160.0(8)	130(4)	840	0.05	638(3)
11	10.12(5)	199(2)	320	0.0012	0
12	20.5(1)	199(2)	504	0.0025	0
13	42.6(2)	199(2)	432	0.005	0
14	83.5(4)	199(2)	432	0.01	0
15	20.4(1)	199(2)	936	0.005	80.5(4)
16	40.85(2)	199(2)	432	0.01	161.0(8)
17	80.7(4)	199(2)	576	0.005	80.3(4)
18	80.1(4)	199(2)	480	0.02	320(2)
19	160.2(8)	199(2)	1200	0.05	640(3)

[a] Estimated uncertainty in parentheses.

3. Retrieval of broadening coefficients and their temperature dependence exponents

3.1. Fitting procedure

The CH_4-N_2 collisional half widths were measured using a multi-spectrum non-linear least squares fitting program [14, 15]. The CH_4 manifolds were successively treated, all the spectra available for each of them being fitted simultaneously. The measurements typically involved the simultaneous adjustment of 17 to 27 observed spectra for each manifold. Each calculated spectrum was computed as the convolution of a monochromatic transmission spectrum with an instrument line shape function, which includes the effects of the finite maximum optical path difference and of the finite source aperture diameter of the interferometer. The background in each spectrum was represented by a polynomial expansion up to the second order (a constant or a linear function was however found to be sufficient in most cases), and the profile of the lines was modeled using a Voigt function with Gaussian width always held fixed to the value calculated for the Doppler broadening. Line intensities were fixed to the values calculated by Boudon et al. [16] and listed in the HITRAN database [17]. Pressure-induced line shift was not needed to fit the spectra to the noise level and line-mixing effects were neglected. The temperature dependent pressure induced widths of the methane lines were modeled according to the following expression:

$$\gamma_L = P_{tot}\left[\gamma_{N_2}\left(\frac{T_0}{T}\right)^{n_{N_2}}(1-x) + \gamma_{\text{self}}\left(\frac{T_0}{T}\right)^{n_{\text{self}}}x\right] \quad (1)$$

where P_{tot} is the total sample pressure, $T_0 = 296\,\text{K}$, T is the temperature (in K) and x is the methane mole fraction (*i.e.* the ratio of the methane to total pressure). γ_{N_2} and γ_{self} are the N_2

and self broadening coefficients at T_0, respectively. n_{N_2} and n_{self} are their respective unitless temperature dependence exponents. Examples of best fits are given in Fig. 1 and Fig. 2 for the $R(6)$ and $R(12)$ lines.

The parameters presented in this paper were retrieved from multispectrum non-linear fits. The fit was first performed on pure methane spectra data at room temperature and then integrating the low temperatures (spectra 1-5, 11-14 in Table 1). Finally, when the fit was satisfactory, the data with the nitrogen mixture were integrated (spectra 6-10, 15-19 in Table 1). All parameters remained free and were calculated simultaneously.

Water vapor lines overlap some of the CH_4 manifolds. For example, H_2O lines measured at 73.2622 cm^{-1} and 124.6536 cm^{-1} are very close to the *R(6)* and *R(11)* manifolds, respectively. Fig. 4 illustrates the latter situation. The positions and intensities of these water vapor lines were fixed to the values available in the HITRAN database [12], while the H_2O mole fraction and an effective broadening parameter of these lines were fitted.

The N_2 and self broadening coefficients and their temperature dependence exponents measured in this work are reported in Table 2. They concern 45 lines belonging to the *R(6)* to *R(12)* manifolds of $^{12}CH_4$. For data that could not be fitted, HITRAN values were taken, and are given without uncertainty.

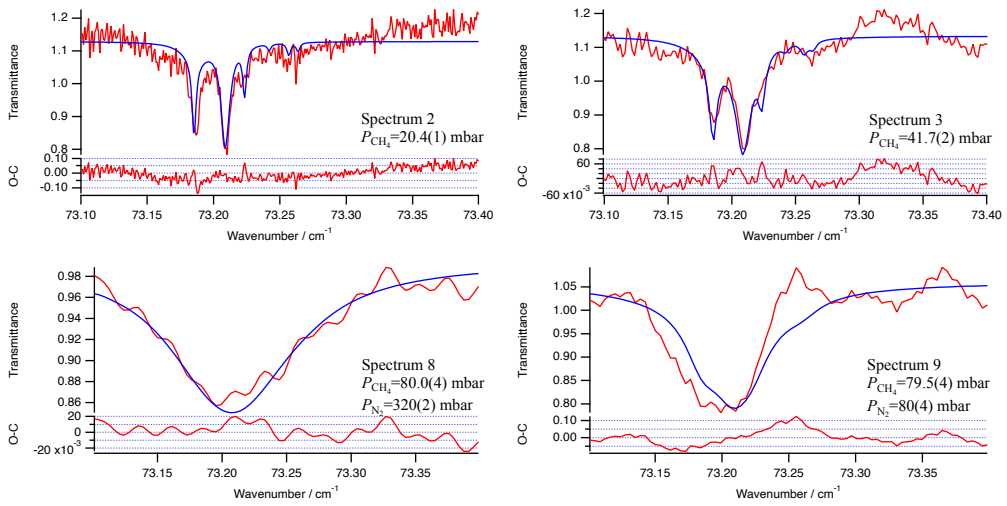

Figure 1: Multispectrum non-linear fit of the $R(6)$ manifold: the 4 observed spectra, in red, (see Table 1) included in the fit, in blue, are overlaid with the corresponding best-fit calculated spectra and residuals (lower pannels).

3.2. Uncertainty estimation

Estimating the accuracy of the measured broadening coefficients requires considering the uncertainties on the physical parameters, contributions from possible systematic errors as well as the uncertainties derived from the fits, taken as the standard deviation. The dominant contributions to the systematic errors (ε_{sys}) arise from the location of the full-scale photometric level, channeling, electronic and detector nonlinearities. An arbitrary value of 5% has been retained for ε_{sys}, much greater than the 2% value in a recent study [18] given the lesser stability of the long path measurements at cryogenic temperatures. Upper limits of the overall relative uncertainties

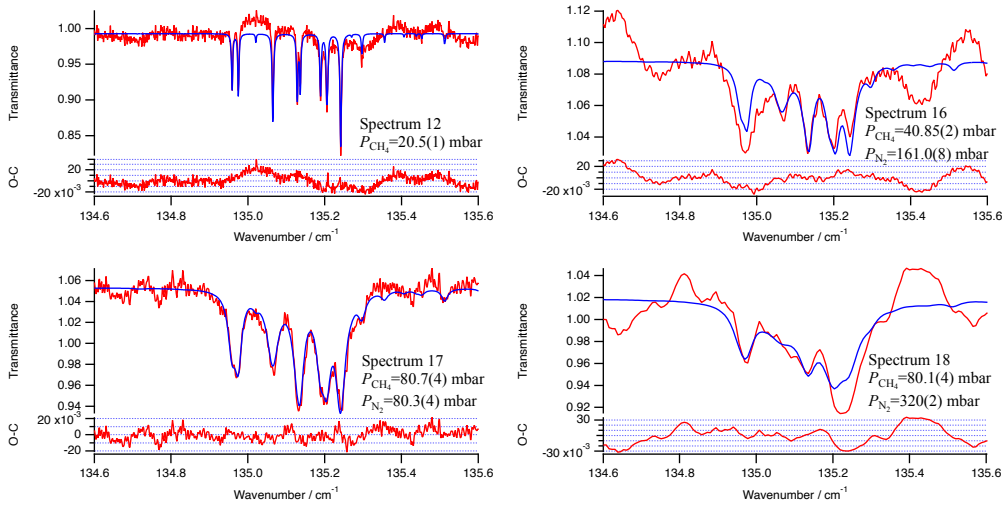

Figure 2: Multispectrum non-linear fits of $R(12)$ lines (see Table 1 for experimental conditions).

on the measured parameters $\varepsilon^{rel}_{\text{total}}$ were calculated as the sum in quadrature (thus assuming they are uncorrelated) of the maximum relative uncertainties on the individual experimental parameters, *i.e.* ε_{si} (sample purity, 0.1%), ε_{T} (temperature, ranging from 3.5 % at 120 K to 1% at 200 K, except for spectra 4 and 5 where uncertainties were estimated to 8%), ε_{p} (pressure, 0.5%), ε_{pl} (pathlength, 0.01%), ε_{fit} (standard deviation from the fit, given for each coefficient in Table 2). The estimated overall uncertainties $\varepsilon_{\text{total}}$ listed in Table 2 were then calculated as the product of $\varepsilon^{rel}_{\text{total}}$ with the corresponding parameter. For the sake of simplicity, and because the difference would be relatively small, we have used the upper limit of ε_{T} = 3.5% for all coefficients.

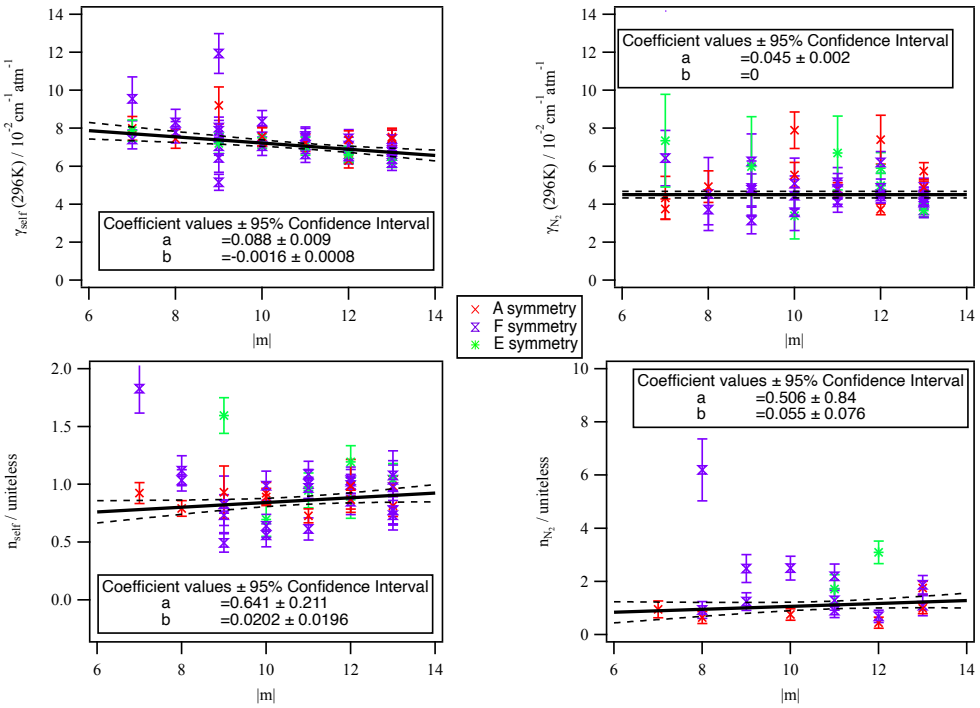

Figure 3: Evolution with $|m|$ (where $m = J'' + 1$ for R-branch lines) of self and N_2 broadening parameters and temperature dependence exponents. Different symbols and colors are used for the A-, E- and F-species transitions. Weighted fits were performed on each set of data points to obtain coefficients used in section 6. One data point is excluded from the plot of γ_{N_2} at $|m| = 7$ for a better visualization.

Table 2: Measured N_2 and self broadening coefficients and temperature exponents for pure rotational lines of $^{12}CH_4$ in natural abundance. The line positions are expressed in cm^{-1}, while line intensities are in $10^{-25} cm^{-1}/(molecule\,cm^{-2})$ at 296 K. For data that could not be fitted, HITRAN values were taken, and are given without uncertainty. The last six columns give the line assignments (using $''$ for the lower sates and $'$ for the upper states).

Position	Intensity	Temperature used (K)	γ_{N_2}	ε_{fit}	ε_{total}	n_{N_2}	ε_{fit}	ε_{total}	γ_{self}	ε_{fit}	ε_{total}	n_{self}	ε_{fit}	ε_{total}	J'	C'	α'	J''	C''	α''
73.186 198	0.9201	120/200/298	0.379 50	0.150 00	0.151 79	0.700			0.095 47	0.010 00	0.011 58	1.830	0.180	0.212	7	F_2	1	6	F_1	1
73.208 941	2.0010	120/200/298	0.043 27	0.011 00	0.011 31	0.952	0.31	0.32	0.079 92	0.003 90	0.006 26	0.924	0.070	0.090	7	A_2	1	6	A_1	1
83.569 132	1.3050	120/200/298	0.045 34	0.019 00	0.019 20	6.420	1.10	1.16	0.083 10	0.004 70	0.006 93	1.120	0.110	0.130	8	F_1	1	7	F_2	2
83.576 220	2.8620	120/200/298	0.049 20	0.007 70	0.008 27	0.638	0.22	0.22	0.074 46	0.002 10	0.005 02	0.792	0.048	0.068	8	A_1	1	7	A_2	1
83.607 176	1.8830	120/200/298	0.036 96	0.007 60	0.008 03	0.926	0.31	0.32	0.077 91	0.002 90	0.005 58	1.040	0.067	0.092	8	F_2	1	7	F_1	2
93.915 549	1.6450	120/200/298	0.062 55	0.014 00	0.014 51	2.480	0.50	0.52	0.080 24	0.002 60	0.005 57	0.732	0.076	0.088	9	F_2	1	8	F_1	2
93.931 069	2.0780	120/200/298	0.047 57	0.007 90	0.008 42	1.240	0.32	0.33	0.070 53	0.001 90	0.004 72	0.830	0.061	0.079	9	F_1	1	8	F_2	1
93.977 670	1.7380	120/200/298	0.059 84	0.026 00	0.026 26	0.690			0.071 78	0.003 00	0.005 34	1.600	0.120	0.155	9	E	1	8	E	2
93.978 997	2.1910	120/200/298	0.048 47	0.014 00	0.014 31	0.690			0.078 78	0.002 60	0.005 48	0.494	0.073	0.079	9	F_1	2	8	F_2	2
94.028 716	0.4316	120/200/298	0.056 00			0.690			0.065 72	0.006 60	0.007 60	0.827	0.240	0.245	9	F_1	3	8	F_2	2
94.142 465	0.5664	120/200/298	0.053 00			0.690			0.092 82	0.008 00	0.009 71	0.931	0.220	0.227	9	A_2	1	8	A_1	1
104.224 694	3.2380	120/200/298	0.078 93	0.008 30	0.009 61	0.650			0.075 31	0.001 80	0.004 95	0.922	0.076	0.095	10	A_2	1	9	A_1	1
104.247 364	2.1690	120/200/298	0.050 87	0.013 00	0.013 37	0.650			0.070 59	0.002 30	0.004 90	0.989	0.110	0.126	10	F_2	1	9	F_1	2
104.252 281	1.6420	120/200/298	0.033 89	0.012 00	0.012 18	0.650			0.074 97	0.003 20	0.005 60	0.695	0.140	0.146	10	E	1	9	E	1
104.315 064	2.7660	120/200/298	0.035 76	0.009 40	0.009 65	2.500	0.42	0.45	0.083 64	0.002 60	0.005 74	0.641	0.092	0.100	10	F_2	2	9	F_1	3
104.319 236	2.5500	120/200/298	0.044 54	0.010 00	0.010 37	0.650			0.075 66	0.002 40	0.005 22	0.560	0.093	0.099	10	F_1	1	9	F_2	2
104.350 038	5.5390	120/200/298	0.055 40	0.005 60	0.006 55	0.758	0.21	0.22	0.075 63	0.001 40	0.004 84	0.890	0.050	0.074	10	A_1	1	9	A_2	1
114.523 421	2.2260	120/200/298	0.051 53	0.007 10	0.007 77	2.190	0.44	0.46	0.071 27	0.001 50	0.004 62	1.000	0.110	0.126	11	F_2	1	10	F_1	1
114.535 302	2.5860	120/200/298	0.040 96	0.004 60	0.005 24	1.290	0.36	0.37	0.066 18	0.001 20	0.004 23	1.090	0.091	0.113	11	F_1	1	10	F_2	2
114.614 369	1.8140	120/200/298	0.066 97	0.019 00	0.019 44	1.710	0.53	0.54	0.070 56	0.002 00	0.004 76	0.948	0.140	0.152	11	E	1	10	E	2
114.617 121	2.8020	120/200/298	0.048 09	0.007 60	0.008 15	0.640			0.075 05	0.001 50	0.004 83	0.614	0.089	0.097	11	F_2	2	10	F_1	2
114.639 394	6.9310	120/200/298	0.047 96	0.001 70	0.003 39	0.640			0.072 37	0.000 84	0.004 51	0.728	0.040	0.060	11	A_2	1	10	A_1	1
114.650 565	2.3870	120/200/298	0.037 45	0.004 80	0.005 32	0.700			0.085 00						7	A_2	2	6	A_1	1
114.671 461	3.5380	120/200/298	0.047 60	0.003 90	0.004 87	0.902	0.26	0.27	0.075 98	0.001 10	0.004 78	0.970	0.071	0.093	11	F_1	2	10	F_2	3
114.926 380	1.4430	120/200/298	0.064 24	0.014 00	0.014 54	0.700			0.074 09	0.002 10	0.005 00				7	F_2	5	6	F_1	2
114.976 348	1.0100	120/200/298	0.073 41	0.024 00	0.024 42	0.700			0.078 79	0.003 00	0.005 68				7	E	4	6	E	2
124.762 736	1.5340	200/298	0.058 95	0.007 40	0.008 23	0.640			0.065 71	0.001 20	0.004 20	0.866	0.150	0.159	12	E	1	11	E	1
124.771 153	2.3700	200/298	0.045 21	0.003 80	0.004 70				0.066 32	0.000 91	0.004 16	0.850	0.100	0.113	12	F_1	1	11	F_2	2
124.783 879	4.2670	200/298	0.037 25	0.001 70	0.002 85	0.447	0.21	0.21	0.062 96	0.000 61	0.003 90	0.867	0.062	0.082	12	A_1	1	11	A_2	1
124.866 856	2.6380	200/298	0.062 00	0.004 30	0.005 74				0.074 67	0.000 91	0.004 66	1.040	0.094	0.113	12	F_1	2	11	F_2	3
124.881 719	0.8196	200/298	0.031 47	0.006 70	0.006 97	0.690			0.051 50	0.002 80	0.004 22				9	F_2	3	8	F_1	2
124.881 895	0.8951	200/298	0.068 00			0.690			0.119 40	0.007 50	0.010 47				9	F_1	3	8	F_2	2
124.909 811	3.7530	200/298	0.044 04	0.002 20	0.003 48	0.686	0.23	0.23	0.065 28	0.000 64	0.004 05	0.994	0.069	0.092	12	F_2	1	11	F_1	2
124.953 539	2.2530	200/298	0.049 81	0.005 70	0.006 47	3.090	0.38	0.42	0.066 25	0.000 98	0.004 17	1.190	0.120	0.141	12	E	2	11	E	2
124.958 857	3.1670	200/298	0.048 61	0.003 60	0.004 67				0.070 90	0.000 81	0.004 42	1.020	0.083	0.104	12	F_2	2	11	F_1	3
125.281 451	1.0670	200/298	0.074 04	0.012 00	0.012 83				0.073 73	0.001 80	0.004 86	0.986	0.220	0.228	12	A_1	2	11	A_2	1
134.958 636	2.0730	200/298	0.049 01	0.003 50	0.004 61	0.630			0.065 42	0.000 83	0.004 09	0.733	0.120	0.128	13	F_2	1	12	F_1	2
134.974 968	2.1490	200/298	0.036 82	0.002 40	0.003 29	0.630			0.061 72	0.000 76	0.003 86	0.777	0.120	0.129	13	F_1	1	12	F_2	1
135.064 743	3.8510	200/298	0.057 42	0.002 70	0.004 43	1.750	0.23	0.25	0.075 41	0.000 63	0.004 66	0.814	0.078	0.093	13	A_1	1	12	A_2	1
135.128 296	2.7510	200/298	0.044 96	0.003 10	0.004 15	1.870	0.33	0.35	0.068 34	0.000 74	0.004 25	1.040	0.110	0.127	13	F_1	2	12	F_2	2
135.136 144	2.2070	200/298	0.036 66	0.002 80	0.003 59	0.630			0.063 17	0.000 80	0.003 95	1.040	0.120	0.136	13	E	1	12	E	2
135.188 872	2.5250	200/298	0.043 72	0.003 00	0.004 02	1.090	0.37	0.38	0.074 36	0.000 83	0.004 63	0.773	0.110	0.120	13	F_1	3	12	F_2	3
135.205 313	2.7630	200/298	0.041 07	0.002 50	0.003 55	0.630			0.067 56	0.000 85	0.004 22	1.080	0.110	0.128	13	F_2	2	12	F_1	3
135.241 444	5.2210	200/298	0.048 82	0.001 60	0.003 39	0.987	0.19	0.20	0.074 55	0.000 54	0.004 60	0.984	0.061	0.086	13	A_2	1	12	A_1	2
135.296 672	0.7780	200/298	0.040 80	0.007 50	0.007 91	0.630			0.063 80	0.001 80	0.004 30	0.974	0.310	0.316	13	F_1	3	12	F_2	2

4. Rotational dependence of the measured parameters

The measured self and N_2 broadening coefficients and their temperature dependence exponents are plotted in Fig. 3 as a function of $|m|$ ($m = J'' + 1$ for R-branch lines, J'' being the lower state rotational quantum number). Different markers and colors are used to distinguish the A-, E- and F-species transitions, showing no emerging trend with symmetry. All the measured quantities were therefore fitted to the following polynomial expansion

$$y = a + b\,|m|, \tag{2}$$

each measured value being weighted according to the inverse of the square of its estimated overall uncertainty. The values of the fitted coefficients a and b obtained are provided in Table 3. Five outliers, $\gamma_{\mathrm{self}} = 0.1194(75)\,\mathrm{cm^{-1}\,atm^{-1}}$ at $|m| = 9$, $\gamma_{\mathrm{N_2}} = 0.38(15)\,\mathrm{cm^{-1}\,atm^{-1}}$ at $|m| = 7$, $n_{\mathrm{self}} = 1.83(21)$ at $|m| = 7$, $n_{\mathrm{self}} = 1.60(15)$ at $|m| = 9$ and $n_{\mathrm{N_2}} = 6.4(11)$ at $|m| = 8$, are off scale. These data were excluded from the polynomial fits. The dispersion of the measured N_2 broadening is larger than that obtained for self broadening, most probably because the stability of the cell optics is more affected at the higher pressures used for N_2 broadening retrieval (minute shifts in the multipass optics occurred unavoidably after filling the cell with the warm gas mixtures). As a results shifts and channelling in the baseline increase the uncertainty in the line fitting. The same comment applies to N_2 temperature dependence exponents. Actually, even if a linear trend emerges, it is difficult to assert it with certainty, especially for $n_{\mathrm{N_2}}$.

Table 3: Values of the fitted coefficients a and b obtained with the polynomial expression $y = a + b\,|m|$.

y	a[a]	b[a]
$\gamma_{\mathrm{self}}/\mathrm{cm^{-1}\,atm^{-1}}$	0.088(9)	−0.0016(8)
$\gamma_{\mathrm{N_2}}/\mathrm{cm^{-1}\,atm^{-1}}$	0.045(2)	0[b]
n_{self}/unitless	0.641(211)	0.0202(196)
$n_{\mathrm{N_2}}$/unitless	0.506(840)	0.0554(760)

[a] Estimated uncertainty in parentheses.

[b] Parameter not fitted.

5. Discussion

To the best of our knowledge, the present work involves the first measurements of N_2 broadening coefficients and their temperature dependence exponents for pure rotational lines of $^{12}CH_4$ at low temperature. So far, there are values of γ_{air} reported in HITRAN that come from references [13, 19, 20]. In addition, measurements were performed in the ν_4 band by Smith et al. [21] for air-broadened half widths, pressure-induced shifts and temperature dependence over a

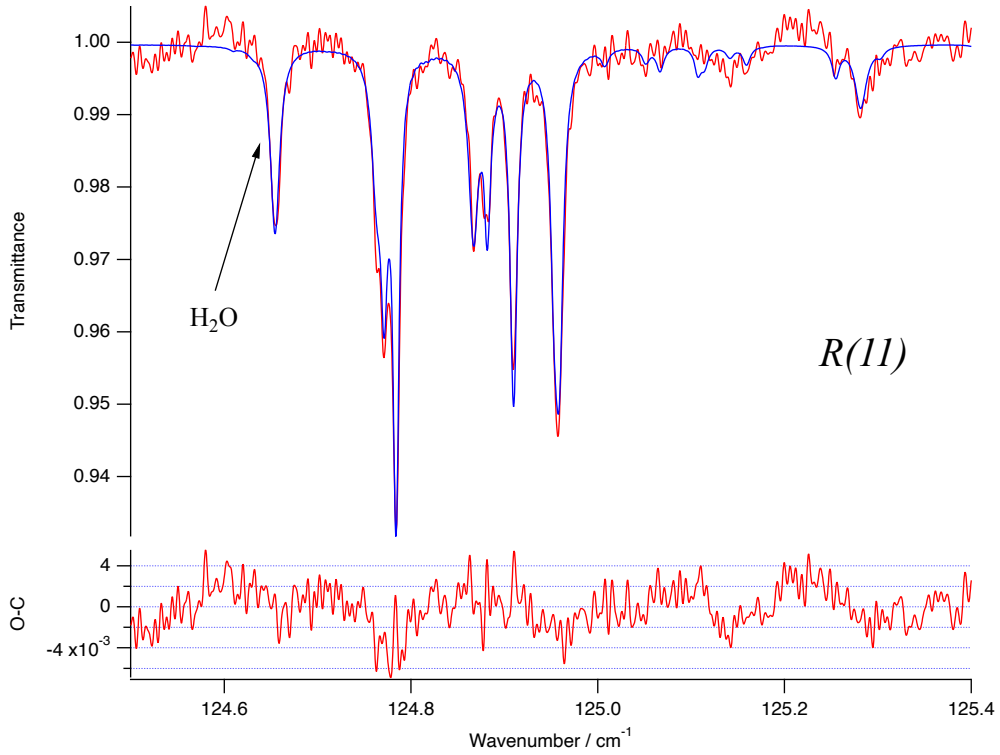

Figure 4: Analysis of the *R(11)* region of the far-infrared spectrum of $^{12}CH_4$, taken at room temperature with a mixture of nitrogen at 133 mbar (see Ref. [13]). The observed spectrum is shown in the upper part, in red and the fitted spectrum in blue. The fit residuals are presented in the lower panel. A water vapor line, included in the fit, is also identified.

wide range of rotational levels. Similarly, the values used in HITRAN for n_{N_2} are estimated temperature exponents described in Ref. [19] and Ref. [20].

Our results can thus be compared to the previous ones for ν_4 and to those used in HITRAN, as performed in Fig. 5. While our data appear to suffer from significant deviation due to the difficulty of achieving the stability of the cell optics, and even though we had to remove one (obviously outlier, see Fig. 3) datum point in each graph for better visualization, the comparison shows a good agreement between air-width parameters and our N_2 parameters, even though with regard to the temperature dependence coefficients, it is more difficult to judge the quality of the comparison. Finally, as already outlined, we find no correlation between the values of the coefficients and the type of symmetry of the lines as illustrated in Fig. 3.

6. Application to analysis of Titan's spectra

We applied the measured broadening coefficients to an analysis of CH_4 rotational lines observed on Titan by the Cassini Composite InfraRed Spectrometer (CIRS) in the 70–150 cm^{-1} wavenumber range, aiming at deriving the stratospheric CH_4 volume mixing ratio (VMR) following the pioneering investigation of Lellouch et al. [2]. We used a selection of Focal Plane 1

(FP1) spectra recorded on February 1st 2016 during the T116 flyby, with the field of view (FOV) centered in a latitude range of 0.5°S – 0.5°N. The selection consists of 204 spectra having a mean latitude of 0.4°N, a FOV of about 20° in latitude, and a mean emission angle of 43°. The spectral resolution is 0.52 cm^{-1}.

Several methane lines are clearly seen over a continuum arising from the N_2-N_2 and CH_4-N_2 collision-induced absorption (and to a lesser extent from that of CH_4-CH_4 and N_2-H_2) and from the photochemical haze (Fig. 6). The intensity of these rotational lines depends on both stratospheric CH_4 VMR and temperature profiles. In addition, it is thus necessary to use the ν_4 band of methane at 1305 cm^{-1}, which is more sensitive to temperature than to methane abundance. To do so, we made a selection of 453 Focal Plane 4 (FP4) CIRS spectra recorded between latitudes of 5°S and 5°N during the same flyby as the FP1 spectra. Its main emission angle is 32°. We then applied an iterative process to retrieve simultaneously the CH_4 VMR and the temperature profile from the fit of the 70–150 cm^{-1} range and of the ν_4 band spectrum. The inversion algorithm that incorporates a line-by-line radiative transfer code is described in Vinatier et al. [22]. Opacity from the photochemical haze was calculated from the haze extinction profile derived by Vinatier et al. [23] from limb spectra at 5°N acquired on February 1st 2016 with the spectral dependence of Vinatier et al. [24]. The CH_4 line positions, intensities and energy levels come from HITRAN2020 [12] and are similar to those used by Lellouch et al. [2]. The N_2-N_2 collision-induced absorption was taken from Gordon et al. [12], as calculated from the trajectory-based approach of Chistikov et al. [25], and that of CH_4-N_2 comes from the new semi-empirical model presented in Finenko et al. [26]. For the room-temperature N_2 broadening coefficients and temperature exponent of the CH_4 lines, we used the $|m|$ dependence given by the polynomial fits in Table 3.

In a first step, we determined the temperature profile assuming an initial CH_4 VMR equal to 1.48%, as measured by the Huygens GCMS [27], and taking the temperature profile of Vinatier et al. [23] derived from CIRS spectra recorded near 0°N on February 1st 2016 as an *a priori* in the inversion process. We fitted the ν_4 CH_4 band centered at 1305 cm^{-1} to infer stratospheric temperatures and the 70–280 cm^{-1} range to infer tropospheric ones (from the collision-induced continuum excluding the CH_4 rotational lines in this step). We then obtained a new temperature profile that was used, in a second step, to fit the CH_4 rotational lines in the 70–150 cm^{-1} spectral range. The derived CH_4 mixing ratio was then used as an input of a new iteration to retrieve the temperature profile in a first step and the CH_4 VMR in a second step. After a few iterations, we obtained convergence of both temperature and CH_4 abundance.

Fig. 6 shows the fit of the CH_4 rotational lines using the line broadening measurements presented here. The retrieved CH_4 VMR is (1.17 ± 0.08)%. This value pertains to a region in the lower stratosphere centered at 85 km (15 mbar) [2]. The inferred VMR is very close to the one obtained when the air-broadening coefficients from HITRAN2020 (based on values from other vibrational CH_4 bands) are used instead: 1.18% with similar error bars. We can also note that the VMR we inferred agrees within error bars with that derived at the equator by Lellouch et al. [2] from Cassini/CIRS nadir spectra recorded on December 5th 2008, (1.00 ± 0.10)%, more than 7 years before the data analyzed here.

7. Conclusion

Multi-spectrum analyses of pure rotational transitions of methane have been performed for pure and nitrogen diluted gas mixing at low temperature. These are the first results of this type

and may be of great interest for the study of the radiative transfer of atmospheres such as Titan. The N_2 broadening parameters are in agreement with air broadening coefficients, obtained from other bands, reported in previous studies. This is less true for the temperature dependence exponents for which higher discrepancies are observed. Nevertheless, these measurements have been applied to observed spectra on Titan by the Cassini Composite InfraRed Spectrometer. Although the results do not show a big difference between these calculations and those made with the values already present in HITRAN, it is a valuable addition to the methane databases.

The measurement of hydrogen broadening parameters is a future experimental prospect in order to better characterize atmospheres that are mainly composed of hydrogen such as the giant planets Neptune and especially Uranus which should be visited by a space probe in a not too distant future.

Finally, these results should be integrated very soon into the database of the Dijon group [28], which can be downloaded at `https://vamdc.icb.cnrs.fr/PHP/methane.php` and is also available through the VAMDC infrastructure [29–32].

Acknowledgments

We acknowledge support from Synchrotron SOLEIL (projects 99180032 and 2019 0174) which enabled us to carry out these experiments. We acknowledge support from the French "Programme National de Planétologie" of INSU/CNRS.

References

[1] E. Lellouch, S. Vinatier, R. Moreno, M. Allen, S. Gulkis, P. Hartogh, J.-M. Krieg, A. Maestrini, I. Mehdi, and A. Coustenis. Sounding of Titan's atmosphere at submillimeter wavelengths from an orbiting spacecraft. *Planetary and Space Science*, 58(13):1724–1739, 2010.

[2] E. Lellouch, B. Bézard, F. M. Flasar, S. Vinatier, R. Achterberg, C. A. Nixon, G. L. Bjoraker, and N. Gorius. The distribution of methane in Titan's stratosphere from Cassini/CIRS observations. *Icarus*, 231:323–337, 2014.

[3] J. W. Barnes, E. P. Turtle, M. G. Trainer, R. D. Lorenz, S. M. MacKenzie, W. B. Brinckerhoff, M. L. Cable, Carolyn M. Ernst, C. Freissinet, K. P. Hand, et al. Science goals and objectives for the Dragonfly Titan rotorcraft relocatable lander. *The Planetary Science Journal*, 2(4):130, 2021.

[4] National Academies of Sciences, Engineering, Medicine, et al. Origins, Worlds, and Life: A Decadal Strategy for Planetary Science and Astrobiology 2023-2032. 2022.

[5] L. A. Sromovsky and P. M. Fry. The methane abundance and structure of Uranus' cloud bands inferred from spatially resolved 2006 Keck grism spectra. *Icarus*, 193(1):252–266, 2008.

[6] G. S. Orton, T. Encrenaz, C. Leyrat, R. Puetter, and A. J. Friedson. Evidence for methane escape and strong seasonal and dynamical perturbations of Neptune's atmospheric temperatures. *Astronomy & Astrophysics*, 473(1): L5–L8, 2007.

[7] E. Lellouch, P. Hartogh, H. Feuchtgruber, B. Vandenbussche, Th. de Graauw, R. Moreno, C. Jarchow, T. Cavalié, G. S. Orton, M. Banaszkiewicz, et al. First results of Herschel-PACS observations of Neptune. *Astronomy & Astrophysics*, 518:L152, 2010.

[8] V. Boudon, O. Pirali, P. Roy, J.-B. Brubach, L. Manceron, and J. Vander Auwera. The high-resolution far-infrared spectrum of methane at the SOLEIL synchrotron. *Journal of Quantitative Spectroscopy and Radiative Transfer*, 111:1117–1129, 2010.

[9] P. Roy, J.-B. Brubach, M. Rouzières, O. Pirali, F. Kwabia Tchana, and L. Manceron. AILES: La ligne infrarouge et THz sur rayonnement synchrotron SOLEIL. *Revue de l'électricité et de l'électronique*, 2008(3):23–30, 2008.

[10] J.-B. Brubach, L. Manceron, M. Rouzières, O. Pirali, D. Balcon, F.K. Tchana, V. Boudon, M. Tudorie, T. Huet, A. Cuisset, and P. Roy. Performance of the AILES THz-infrared beamline on SOLEIL for high resolution spectroscopy. *AIP Conference Proceeding*, 1214:81–84, 2010.

[11] F. Kwabia Tchana, F. Willaert, X. Landsheere, J.-M. Flaud, L. Lago, M. Chapuis, C. Herbeaux, P. Roy, and L. Manceron. A new, low temperature long-pass cell for mid-infrared to terahertz spectroscopy and synchrotron radiation use. *Review of Scientific Instruments*, 84(9):093101, 2013.

[12] I. E. Gordon, L. S. Rothman, R. J. Hargreaves, R. Hashemi, E. V. Karlovets, F. M. Skinner, E. K. Conway, C. Hill, R. V. Kochanov, Y. Tan, et al. The HITRAN2020 molecular spectroscopic database. *Journal of quantitative spectroscopy and radiative transfer*, 277:107949, 2022.

[13] M. Sanzharov, J. Vander Auwera, O. Pirali, P. Roy, J.-B. Brubach, L. Manceron, T. Gabard, and V. Boudon. Self and N_2 collisional broadening of far-infrared methane lines measured at the SOLEIL synchrotron. *Journal of Quantitative Spectroscopy and Radiative Transfer*, 113(15):1874–1886, 2012.

[14] M. Tudorie, T. Földes, A. C. Vandaele, and J. Vander Auwera. CO_2 pressure broadening and shift coefficients for the 1–0 band of HCl and DCl. *Journal of Quantitative Spectroscopy and Radiative Transfer*, 113(11):1092–1101, 2012.

[15] L. Daneshvar, T. Földes, J. Buldyreva, and J. Vander Auwera. Infrared absorption by pure CO_2 near 3340 cm^{-1}: Measurements and analysis of collisional coefficients and line-mixing effects at subatmospheric pressures. *Journal of Quantitative Spectroscopy and Radiative Transfer*, 149:258–274, 2014.

[16] V. Boudon, O. Pirali, P. Roy, J.-B. Brubach, L. Manceron, and J. Vander Auwera. The high-resolution far-infrared spectrum of methane at the SOLEIL synchrotron. *Journal of Quantitative Spectroscopy and Radiative Transfer*, 111(9):1117–1129, 2010.

[17] L. R. Brown, K. Sung, D. C. Benner, V. M. Devi, V. Boudon, T. Gabard, C. Wenger, A. Campargue, O. Leshchishina, S. Kassi, et al. Methane line parameters in the HITRAN2012 database. *Journal of Quantitative Spectroscopy and Radiative Transfer*, 130:201–219, 2013.

[18] Y. Attafi, A. B. Hassen, H. Aroui, F. Kwabia Tchana, L. Manceron, D. Doizi, J. Vander Auwera, and A. Perrin. Self and N_2 collisional broadening of rovibrational lines in the ν_6 band of methyl iodide ($^{12}CH_3I$) at room temperature: The *J* and *K* dependence. *Journal of Quantitative Spectroscopy and Radiative Transfer*, 231:1–8, 2019.

[19] L. R. Brown, D. C. Benner, J.-P. Champion, V. M. Devi, L. Fejard, R. R. Gamache, T. Gabard, J. C. Hilico, B. Lavorel, M. Loë te, et al. Methane line parameters in HITRAN. *Journal of Quantitative Spectroscopy and Radiative Transfer*, 82(1-4):219–238, 2003.

[20] L. R. Brown. Empirical line parameters of methane from 1.1 to 2.1 μm. *Journal of Quantitative Spectroscopy and Radiative Transfer*, 96(2):251–270, 2005.

[21] M. H. Smith, D. C. Benner, A. Predoi-Cross, and V. M. Devi. Multispectrum analysis of $^{12}CH_4$ in the ν_4 band: I.: Air-broadened half widths, pressure-induced shifts, temperature dependences and line mixing. *Journal of Quantitative Spectroscopy and Radiative Transfer*, 110(9-10):639–653, 2009.

[22] S. Vinatier, B. Bézard, S. Lebonnois, N. A. Teanby, R. K. Achterberg, N. Gorius, A. Mamoutkine, E. Guandique, A. Jolly, D. E. Jennings, et al. Seasonal variations in Titan's middle atmosphere during the northern spring derived from Cassini/CIRS observations. *Icarus*, 250:95–115, 2015.

[23] S. Vinatier, C. Mathé, B. Bézard, J. V. d'Ollone, S. Lebonnois, C. Dauphin, F. M. Flasar, R. K. Achterberg, B. Seignovert, M. Sylvestre, et al. Temperature and chemical species distributions in the middle atmosphere observed during Titan's late northern spring to early summer. *Astronomy & Astrophysics*, 641:A116, 2020.

[24] S. Vinatier, P. Rannou, C. M. Anderson, B. Bézard, R. De Kok, and R. E. Samuelson. Optical constants of Titan's stratospheric aerosols in the 70–1500 cm- 1 spectral range constrained by Cassini/CIRS observations. *Icarus*, 219 (1):5–12, 2012.

[25] D. N. Chistikov, A. A. Finenko, S. E. Lokshtanov, S. V. Petrov, and A. A. Vigasin. Simulation of collision-induced absorption spectra based on classical trajectories and ab initio potential and induced dipole surfaces. I. Case study of N_2–N_2 rototranslational band. *The Journal of Chemical Physics*, 151(19):194106, 2019.

[26] A. A. Finenko, B. Bézard, I. E. Gordon, D. N. Chistikov, S. E. Lokshtanov, S. V. Petrov, and A. A. Vigasin. Trajectory-based Simulation of Far-infrared Collision-induced Absorption Profiles of CH_4–N_2 for Modeling Titan's Atmosphere. *The Astrophysical Journal Supplement Series*, 258(2):33, 2022.

[27] H. B. Niemann, S. K. Atreya, J. E. Demick, D. Gautier, J. A. Haberman, D. N. Harpold, W. T. Kasprzak, J. I. Lunine, T. C. Owen, and F. Raulin. Composition of Titan's lower atmosphere and simple surface volatiles as measured by the Cassini-Huygens probe gas chromatograph mass spectrometer experiment. *Journal of Geophysical Research: Planets*, 115(E12), 2010.

[28] C. Richard, V. Boudon, and M. Rotger. Calculated spectroscopic databases for the VAMDC portal: New molecules and improvements. *J. Quant. Spectrosc. Radiat. Transfer*, 251:107096, 2020.

[29] Marie-Lise Dubernet, Vincent Boudon, JL Culhane, MS Dimitrijevic, AZ Fazliev, Christine Joblin, F Kupka, G Leto, Pierre Le Sidaner, PA Loboda, et al. Virtual atomic and molecular data centre. *Journal of Quantitative Spectroscopy and Radiative Transfer*, 111(15):2151–2159, 2010.

[30] Marie-Lise Dubernet, BK Antony, Yaye-Awa Ba, Yu L Babikov, Klaus Bartschat, Vincent Boudon, BJ Braams, Hyun-Kyung Chung, Fabien Daniel, Franck Delahaye, et al. The virtual atomic and molecular data centre (VAMDC) consortium. *Journal of Physics B: Atomic, Molecular and Optical Physics*, 49(7):074003, 2016.

[31] Nicolas Moreau, Carlo-Maria Zwolf, Yaye-Awa Ba, Cyril Richard, Vincent Boudon, and Marie-Lise Dubernet. The VAMDC portal as a major enabler of atomic and molecular data citation. *Galaxies*, 6(4):105, 2018.

[32] D. Albert, B. K. Antony, Y. A Ba, Y. L. Babikov, P. Bollard, V. Boudon, F. Delahaye, G. Del Zanna, M. S. Dim-

itrijević, B. J. Drouin, M.-L. Dubernet, F. Duensing, M. Emoto, C. P. Endres, A. Z. Fazliev, J.-M. Glorian, I. E. Gordon, P. Gratier, C. Hill, D. Jevremović, C. Joblin, D.-H. Kwon, R. V. Kochanov, E. Krishnakumar, G. Leto, P. A. Loboda, A. A. Lukashevskaya, O. M. Lyulin, B. P. Marinković, A. Markwick, T. Marquart, N. J. Mason, C. Mendoza, T. J. Millar, N. Moreau, S. V. Morozov, T. Möller, Holger S. P. Müller, G. Mulas, I. Murakami, Y. Pakhomov, P. Palmeri, J. Penguen, V. I. Perevalov, N. Piskunov, J. Postler, A. I. Privezentsev, P. Quinet, Y. Ralchenko, Y.-J. Rhee, C. Richard, G. Rixon, L. S. Rothman, E. Roueff, T. Ryabchikova, S. Sahal-Bréchot, P. Scheier, P. Schilke, S. Schlemmer, K. W. Smith, B. Schmitt, I. Yu. Skobelev, V. A. Srecković, E. Stempels, S. A. Tashkun, J. Tennyson, V. G. Tyuterev, C. Vastel, V. Vujčić, V. Wakelam, N. A. Walton, C. Zeippen, and C. M. Zwölf. A decade with VAMDC: Results and ambitions. *Atoms*, 8:76, 2020.

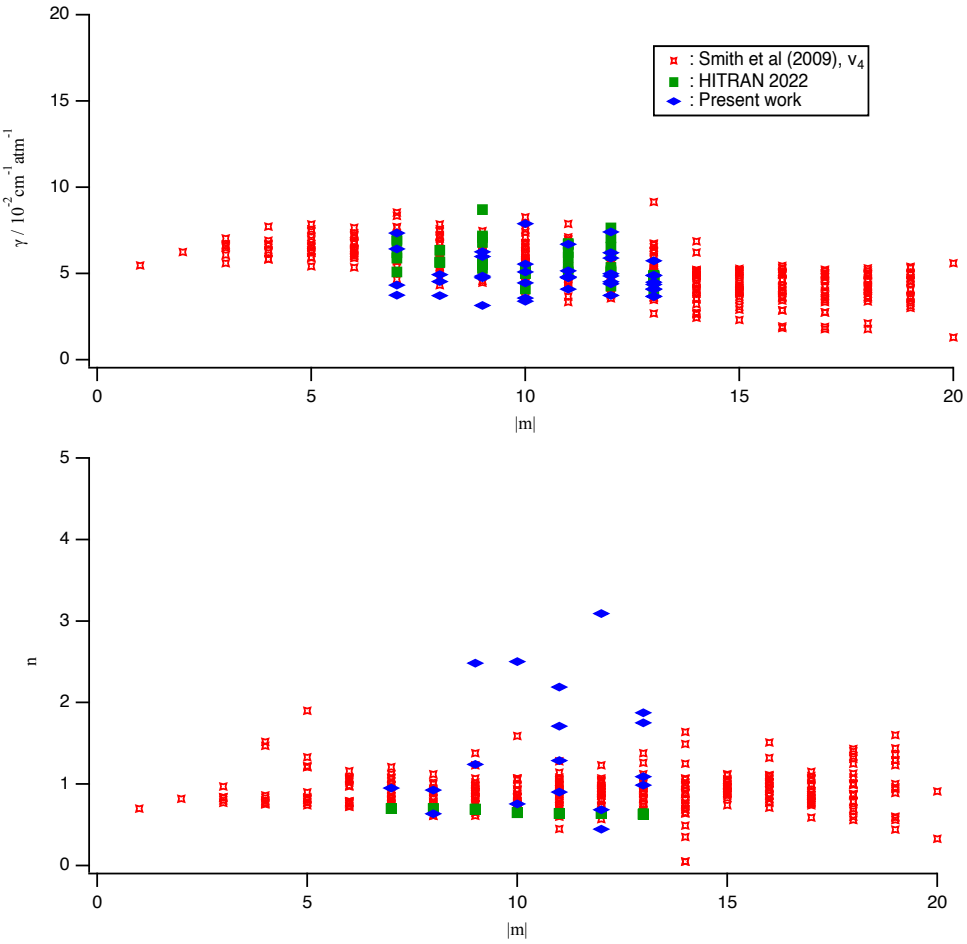

Figure 5: Comparison of our measurements with the ones performed by Smith et al. [21] of air-width and temperature dependence exponents in the ν_4 band and the data found in HITRAN, in the [0, 20] range of $|m|$. One data point of this present work was removed in each graph for better visualization: at $m = |7|$ for the comparison of broadening coefficients, and at $m = |8|$ for the temperature dependence.

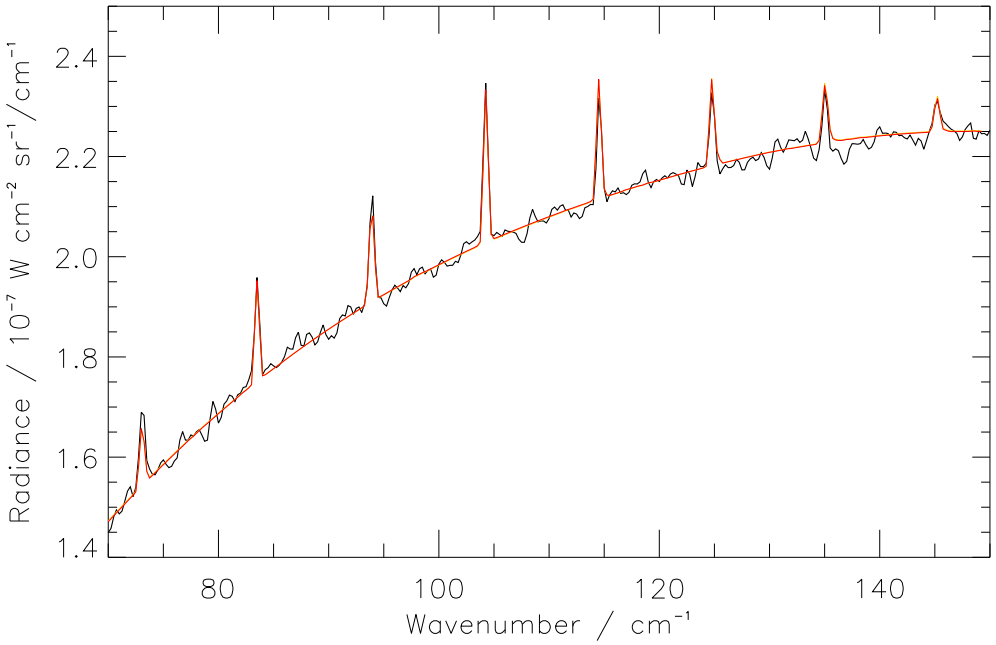

Figure 6: Comparison of a selection of Cassini/CIRS spectra recorded near the equator in February 2016 (black) with a synthetic spectrum calculated with a CH_4 mole fraction of 1.17% in the stratosphere. The temperature profile used in the calculations was derived by fitting the continuum between the CH_4 lines and the methane band observed by Cassini/CIRS around 1305 cm^{-1}. The 1-standard deviation noise level in the observed spectrum is about $7{\times}10^{-10}$ $Wcm^{-2}sr^{-1}/cm^{-1}$ and the spectral resolution is 0.52 cm^{-1}.